*energies*

MDPI

*Article*

# Computational Fluid Dynamics of Ammonia Synthesis in Axial-Radial Bed Reactor

**Mariusz Tyrański [1], Jakub Michał Bujalski [2], Wojciech Orciuch [1] and Łukasz Makowski [1,*]**

[1] Faculty of Chemical and Process Engineering, Warsaw University of Technology, Waryńskiego 1, 00-645 Warsaw, Poland; wojciech.orciuch@pw.edu.pl (W.O.)
[2] Yara International ASA, Yara Technology and Projects, 3936 Porsgrunn, Norway; jakub.bujalski@yara.com
* Correspondence: lukasz.makowski.ichip@pw.edu.pl

**Abstract:** Ammonia synthesis by the Haber–Bosch method is a typical and effective implementation of the chemical process in the large-scale fertiliser industry. Due to the growing demand for fertilisers and food, it is desirable to study this process thoroughly using modern numerical methods to improve the operation of existing devices and facilitate the design of new devices in industrial installations. This manuscript focuses on the influence of the catalyst bed parameters on the ammonia synthesis process. Variants with different sizes of catalyst particles and modifications of the geometry of catalytic beds were considered. The axial-radial Topsoe converter with magnetite as a catalyst, commonly used in modern fertiliser industry beds, was investigated using Computational Fluid Dynamics. As a result, contours of velocity, pressure, concentration, and rate of ammonia formation were obtained. The analysis of the obtained results made it possible to determine the gradient of ammonia production rate in the catalyst bed and designate zones with negligible reaction rates. The authors also proposed possible bed geometry modifications to reduce bed volumes without affecting the converter's performance.

**Keywords:** ammonia synthesis; Haber–Bosch method; axial-radial bed reactor; Topsoe ammonia process; magnetite catalyst beds; computational fluid dynamics; CFD

check for updates

**Citation:** Tyrański, M.; Bujalski, J.M.; Orciuch, W.; Makowski, Ł. Computational Fluid Dynamics of Ammonia Synthesis in Axial-Radial Bed Reactor. *Energies* **2023**, *16*, 6680. https://doi.org/10.3390/en16186680

Academic Editor: Mostafa H. Elsharqawy

Received: 13 August 2023
Revised: 9 September 2023
Accepted: 15 September 2023
Published: 18 September 2023

**Copyright:** © 2023 by the authors. Licensee MDPI, Basel, Switzerland. This article is an open access article distributed under the terms and conditions of the Creative Commons Attribution (CC BY) license (https://creativecommons.org/licenses/by/4.0/).

## 1. Introduction

Large-scale production of fertilisers causes many scientific discussions about their influence on the environment and human health [1,2]. However, the necessity to increase production due to global food insecurity [3] and market analyses [4–7] indicate that the demand for fertilisers will grow. Degradation and ongoing loss of habitats for many species of animals and plants [8] force the search for solutions that increase food production while limiting the growth of agricultural areas, which makes the need to improve the production of fertilisers particularly important nowadays. One way to increase the production of fertilisers is to modernise existing processes. It is faster than developing new technologies and has a better chance of successful implementation in large-scale production, where even a slight improvement can significantly influence the cost of the product.

The Haber–Bosch ammonia synthesis process is currently the most widespread and one of the most efficient methods for large-scale ammonia production [9–11]. This process is one of the main stages of fertiliser production. In a typical Haber–Bosch process, the reaction takes place on a catalytic bed containing magnetite, which generates high and stable activity and is suitable for the large-scale production of ammonia [11]. There are many different commercial approaches to ammonia synthesis. The Kellogg Ammonia process uses centrifugal compressors and a converter containing four axial-flow catalyst beds with an integrated heat recovery system and is characterised by high efficiency [12]. The Braun Purifier Process is based on the steam-reforming route and is characterised by a significant excess of process air. Ammonia synthesis occurs in a 2-stage adiabatic synthesis converter with two-bed axial flow and heat exchange between beds [12]. Currently, the

most widely used solution is the Topsoe Ammonia Process. This process follows the steam-reforming route, and in this case, the most influence on the process is obtained through the selection of the catalyst (its size, shape, porosity, and placement) and the geometry of the catalytic bed. Topsoe's converter usually contains 2–3 beds with the axial-radial flow and is characterised by low pressure drop. This construction allows for smaller catalyst particles, making it possible to obtain a given conversion in smaller volumes of catalyst bed [12].

In the literature, many successful attempts at numerical modelling of ammonia synthesis exist. Singh and Saraf [13] obtained a mathematical model for adiabatic and auto-thermal ammonia synthesis reactors, and their model was used further by Jorqueira et al. [14] for modelling and sensitivity studies of ammonia converters. Elnashaie et al. [15] elaborated a heterogeneous model for steady-state simulation of a countercurrent tube-cooled fixed-bed ammonia reactor coupled to a heat exchanger. Kasiri et al. [16] simulated a four-bed ammonia synthesis reactor in a dynamic environment. Panahandeh et al. [17] developed a two-dimensional model for an axial-radial ammonia synthesis reactor. In their work, the Navier-Stokes and continuity equations were used to model momentum, mass, and energy balance, and the results were consistent with industrial plant data. Dashti et al. [18] developed a one-dimensional and non-homogenous model of the Kellogg ammonia reactor with three axial flow catalyst beds and an internal heat exchanger. Azarhoosh et al. [19] used a genetic algorithm to simulate and optimise a horizontal ammonia synthesis reactor. Many of those studies use Temkin-Pyzhev equation variants for modelling the ammonia synthesis's kinetics. Dyson and Simon developed one of the most versatile kinetic models with diffusion correction [20]. Although current literature contains many attempts at modelling ammonia synthesis reactors, there seems to be little research on the use of Computational Fluid Dynamics (CFD) in this field. Still, Mirvakili et al. [21] successfully simulated a two-dimensional ammonia synthesis reactor using CFD methods and obtained results that coincided with industrial data.

The motivation of this work is to use CFD methods further to improve the work of ammonia synthesis converters. The authors implemented the modified Temkin-Pyzhev expression developed by Dyson and Simon [20], and the examined ammonia synthesis reactor is the Topsoe converter with radial-axial flow through catalyst beds. The investigated catalyst is magnetite, and the influence of different catalyst particle sizes was considered. This work is focused on obtaining contours of velocity, pressure, concentration, and reaction rate to determine the gradient of ammonia production rate in the catalyst bed and designate dead zones with negligible reaction rates. The authors also proposed possible bed geometry modifications to reduce bed volumes without affecting the converter's performance.

## 2. Materials and Methods

### *2.1. Materials and Process Parameters*

The gas mixture and process parameters widely used in industry were considered in the present work [12,17,21,22]. Experimental data published by Panahandeh et al. [17] were applied for calculations, and their results were used as validation. Table 1 presents the composition of the gas mixture at the inlet, and Table 2 contains the process parameters applied at the inlet of the reactor.

**Table 1.** The composition of the inlet gas stream.

| Species Name | Concentration (Mole Fractions) |
|---|---|
| $N_2$ | 0.2093 |
| $H_2$ | 0.6280 |
| $NH_3$ | 0.0347 |
| $CH_4$ (inert) | 0.0939 |
| Ar (inert) | 0.0341 |

**Table 2.** Process parameters applied at the inlet of the reactor.

| Parameter | Value |
|---|---|
| pressure (atm) | 220 |
| temperature (°C) | 342 |
| flow rate (kmol $h^{-1}$) | 19,622.17 |
| flow rate (kg $s^{-1}$) | 57.7154 |
| velocity (m $s^{-1}$) | 6 |

### *2.2. The Computational Domain*

The considered ammonia converter is the Topsoe axial-radial reactor with three catalyst beds. In this work, the first bed of the reactor and its vicinity were simulated. The catalyst bed's geometry was created based on Panahandeh et al. [17], and the vicinity of the bed was modelled based on Mirvakili et al. [21]. The computational domain is two-dimensional and axisymmetric (Figure 1).

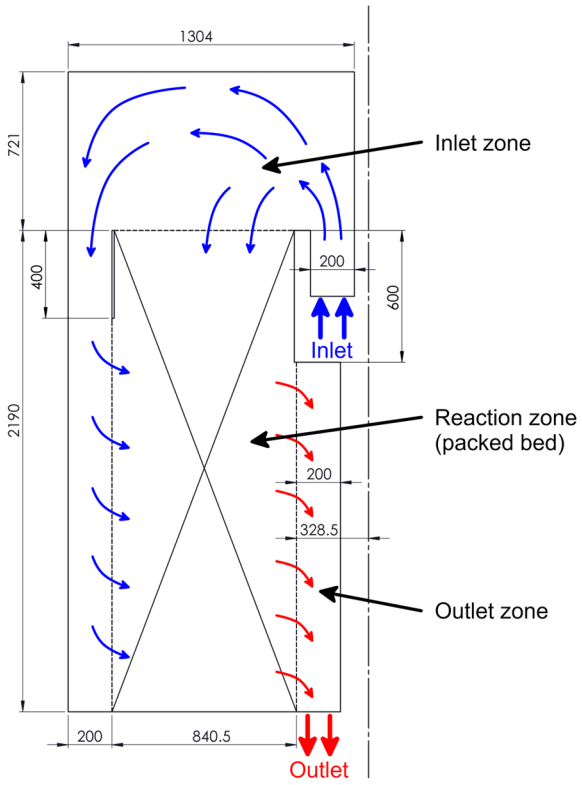



**Figure 1.** Computational domain of the investigated ammonia converter, dimensions in mm. Please note that the arrows indicating the flow direction are for reference only and do not take into account phenomena such as circulation zones.

The catalyst is held inside the annulus-shaped bed. In the inner radius, the converter contains a heat recovery system based on shell-and-tube heat exchangers used to preheat feed gas. The inlet of the feed gas stream is located close to the system's axis. The top part of the catalyst bed (about 400 mm at the outer wall and 600 mm at the inner wall) contains non-perforated walls forcing axial gas flow, while the rest of the catalyst bed's walls are perforated, and the radial gas flow becomes dominant at the middle and lower levels of the bed. After passing through the bed, gas comes out through the inner perforated wall into the inner heat recovery system before entering the second catalyst bed. It should be noted that, due to the very limited data about the converter's geometry in the literature, the computational domain of the catalyst bed's vicinity is simplified, and its dimensions were estimated.

### 2.3. Gas-Phase Modelling

The computational mesh was generated with the Meshing module of the Ansys Workbench 2021 R2, and the number of numerical grids was approximately 90,000 quadrilateral cells. The finest mesh is within the catalyst bed, and the $y^+$ ~1 condition was satisfied by setting the near-wall cell sizes. The system's average turbulence energy dissipation rate and wall shear stress value at the walls were used to check the mesh independence. The meshes were tested until the difference between those two quantities was less than 3% compared to those with a denser mesh. All calculations were conducted in the Ansys Fluent 2021 R2 solver. The SIMPLE method was used for pressure-velocity coupling, and second-order discretisation schemes were used for all variables. The steady-state condition with gravity force was applied. The SST k-ω turbulence model was chosen since it is suitable for predicting heat transfer effects within a packed bed [23,24]. The following equations govern continuity (1) and momentum (2) in the calculations [25]:

$$\frac{\partial \rho}{\partial t} + \nabla \cdot \left( \rho \vec{v} \right) = 0 \tag{1}$$

$$\frac{\partial}{\partial t}\left( \rho \vec{v} \right) + \nabla \cdot \left( \rho \vec{v} \vec{v} \right) = -\nabla p + \nabla \cdot \left\{ \mu \left[ \left( \nabla \vec{v} + \nabla \vec{v}^{T} \right) - \frac{2}{3} \nabla \cdot \vec{v} I \right] \right\} \tag{2}$$

For the SST k-ω model, the turbulent kinetic energy k (3) and the specific dissipation rate ω (4) are calculated from the following equations [25]:

$$\frac{\partial}{\partial t}(\rho k) + \frac{\partial}{\partial x_i}(\rho k u_i) = \frac{\partial}{\partial x_j}\left[ \left( \mu + \frac{\mu_t}{\sigma_k} \right) \frac{\partial k}{\partial x_j} \right] + G_k - Y_k + S_k + G_b \tag{3}$$

$$\frac{\partial}{\partial t}(\rho \omega) + \frac{\partial}{\partial x_i}(\rho \omega u_i) = \frac{\partial}{\partial x_j}\left[ \left( \mu + \frac{\mu_t}{\sigma_\omega} \right) \frac{\partial \omega}{\partial x_j} \right] + G_\omega - Y_\omega + S_\omega + G_{\omega b} \tag{4}$$

Transport of the turbulence shear stress for the SST k-ω model is in the definition of the turbulent viscosity [25]:

$$\mu_t = \frac{\rho k}{\omega} \cdot \frac{1}{\max\left[ \frac{1}{\alpha^*}, \frac{SF_2}{\alpha_1 \omega} \right]} \tag{5}$$

where S is the strain rate magnitude, $\alpha^*$, $\alpha_1$ are coefficients, and $F_2$ is defined as:

$$F_2 = \tanh\left\{ \left[ \max\left( 2\frac{\sqrt{k}}{0.09\omega y}, \frac{500\mu}{\rho y^2 \omega} \right) \right]^2 \right\} \tag{6}$$

where y is the distance to the next surface.

### 2.4. Catalyst Bed Modelling

The flow through the catalyst bed was calculated as a porous zone model. In Fluent, porous media are modelled by adding the momentum source term to the standard fluid flow equations [25]:

$$S_i = -\left( \sum_{j=1}^{3} D_{ij} \mu v_j + \sum_{j=1}^{3} C_{ij} \frac{1}{2} \rho |v| v_j \right) \tag{7}$$

where $S_i$ is the source term for the i (x, y, or z) momentum equation, $|v|$ is the magnitude of the velocity, and C and D are prescribed matrices. This momentum sink contributes to the pressure gradient in the porous cell, making the pressure drop proportional to the fluid velocity in the cell. This source term contains two parts: the first is a viscous loss term (the first term on the right-hand side of Equation (7)), and the second is an inertial loss term (the

second term on the right-hand side of Equation (7)). In the case of simple, homogeneous porous media, the momentum source term is calculated by the following equation:

$$S_i = -\left(\frac{\mu}{\alpha}v_i + C_2\frac{1}{2}\rho|v|v_i\right) \quad (8)$$

where $\alpha$ is the permeability, and $C_2$ is the inertial resistance factor.

The catalyst was considered to be magnetite particles with 1–10 mm diameters (of the equivalent sphere). Modern reactors allow the use of considerably smaller particles (1–2 mm) in high-temperature beds [26,27]. In this work, the influence of catalyst particle size was investigated. The catalyst parameters are listed in Table 3.

**Table 3.** Catalyst parameters.

| Name | Value | Source |
|---|---|---|
| material | magnetite | [11] |
| particle diameter (mm) | vary from 1 to 10 | [26,27] |
| porosity (-) | 0.52 | [27] |
| sphericity (-) | 0.65 | [26] |

The surface-to-volume ratio is an essential parameter of the catalyst bed in the case of porous zone modelling using CFD methods. It was calculated from Equation (9) [26]:

$$S_v = \frac{6}{\psi d_p} \quad (9)$$

where $S_v$ is the surface-to-volume ratio, $\psi$ is the sphericity, and $d_p$ is the particle diameter. Other parameters critical for CFD calculations, such as viscous and inertial resistances, were calculated using the Ergun Equation for packed beds [25]. The viscous resistance (inverse permeability) was calculated from Equation (10):

$$C_1 = \frac{1}{\alpha} = \frac{150}{{d_p}^2}\cdot\frac{(1-\varepsilon)^2}{\varepsilon^3} \quad (10)$$

and the inertial resistance was calculated from Equation (11):

$$C_2 = \frac{3.5}{d_p}\cdot\frac{(1-\varepsilon)}{\varepsilon^3} \quad (11)$$

where $\alpha$ is the permeability, $C_1$ is the viscous resistance, $C_2$ is the inertial resistance, $\varepsilon$ is the porosity, and $d_p$ is the particle diameter (units in meters). Table 4 contains calculated values of surface-to-volume ratios, viscous resistances, and inertial resistances for every considered particle diameter.

In Fluent, fluid flow simulations with porous zones are not assumed to be in thermal equilibrium. Instead, a dual-cell approach is used, where a solid zone is spatially coincident with the porous fluid zone. In this approach, the solid zone only interacts with the fluid concerning heat transfer [25]. The conservation equation for the fluid zone can be written as:

$$\frac{\partial}{\partial t}(\varepsilon\rho_f E_f) + \nabla\cdot\left[\vec{v}(\rho_f E_f + p)\right] = \nabla\cdot\left[\varepsilon k_f \nabla T_f - \left(\sum_i h_i J_i\right) + \left(\bar{\bar{\tau}}\vec{v}\right)\right] + S_f^h + h_{fs}A_{fs}(T_s - T_f) \quad (12)$$

and the conservation equation for the solid zone is expressed as:

$$\frac{\partial}{\partial t}[(1-\varepsilon)\rho_s E_s] = \nabla\cdot[(1-\varepsilon)k_s\nabla T_s] + S_s^h + h_{fs}A_{fs}(T_f - T_s) \quad (13)$$

**Table 4.** Calculated parameters of the catalyst bed for considered catalyst particle diameters for the bed's porosity value of 0.52.

| Particle Diameter (mm) | Surface-to-Volume Ratio ($m^{-1}$) | Viscous Resistance ($m^{-2}$) | Inertial Resistance ($m^{-1}$) |
|---|---|---|---|
| 1 | 9231 | $2.46 \times 10^8$ | 11,948 |
| 1.5 | 6154 | $1.09 \times 10^8$ | 7965 |
| 2 | 4615 | $6.14 \times 10^7$ | 5974 |
| 3 | 3077 | $2.73 \times 10^7$ | 3983 |
| 4 | 2308 | $1.54 \times 10^7$ | 2987 |
| 5 | 1846 | $9.83 \times 10^6$ | 2390 |
| 6 | 1538 | $6.83 \times 10^6$ | 1991 |
| 8 | 1154 | $3.84 \times 10^6$ | 1494 |
| 10 | 923 | $2.46 \times 10^6$ | 1195 |

### *2.5. Reaction Kinetics*

The present work simulates ammonia synthesis reactions using Fluent's Species Transport. In this model, the convection-diffusion equations for each species are solved:

$$\frac{\partial}{\partial t}(\rho Y_i) + \nabla\left(\rho \vec{v} Y_i\right) = -\nabla \vec{J_i} + R_i + S_i \quad (14)$$

In this Equation, the Schmidt number is described by turbulent viscosity and diffusivity. The species' diffusion fluxes are calculated as a temperature and concentration gradient from Fick's law. The ideal gas mixing law was applied to calculate the properties of the gas mixture, and the kinetic theory was used to compute mass diffusivity coefficients.

The ammonia synthesis reaction proceeds as follows:

$$N_2 + 3\,H_2 \rightarrow 2\,NH_3$$

The reaction rate was calculated by the modified Temkin and Pyzhev equation reported by Dyson and Simon [20]:

$$R_{NH_3} = 2k\left[{K_a}^2 a_1 \left(\frac{{a_2}^3}{{a_3}^2}\right)^{\alpha} - \left(\frac{{a_3}^2}{{a_2}^3}\right)^{1-\alpha}\right] \quad (15)$$

The components are designated by subscripts: 1-Nitrogen, 2-Hydrogen, and 3-Ammonia. Parameter $\alpha$ has been set to 0.5 as it fits the experimental data well [20]. The equilibrium constant is calculated from the equation developed by Gillespie and Beattie [28]:

$$\log_{10} K_a = -2.691122 \log_{10} T - 5.519265 \cdot 10^{-5} T + 1.848863 \cdot 10^{-7} T^2 + \frac{2001.6}{T} + 2.6899 \quad (16)$$

The activities are calculated from the following equation:

$$a_i = \frac{f_i}{{f_i}^*} \quad (17)$$

where $f_i$ is the component fugacity and $f_i$* is the fugacity of the component in the chosen standard state. For $f_i$* equal to the pure component fugacity at 1 atm and the temperature of the system, the activities can be calculated as:

$$a_i = f_i = y_i {f_i}^0 \quad (18)$$

where ${f_i}^0$ is the fugacity of the pure component at the temperature and pressure of the system, and it can be calculated using the activity coefficients:

$${f_i}^0 = \gamma_i P \quad (19)$$

The following expressions calculate the activity coefficients for nitrogen, hydrogen, and ammonia [20]:

$$\gamma_1 = 0.93431737 + 0.3101804 \cdot 10^{-3}T + 0.295896 \cdot 10^{-3}P - 0.2707279 \cdot 10^{-6}T^2 + 0.4775207 \cdot 10^{-6}P^2 \quad (20)$$

$$\gamma_2 = \exp\left\{\left[e^{(-3.8402 \cdot T^{0.125} + 0.541)}P - e^{(-0.1263 \cdot T^{0.5} - 15.980)}P^2 + 300\left[e^{(-0.011901T - 5.941)}\right]\left(e^{\frac{-P}{300}} - 1\right)\right]\right\} \quad (21)$$

$$\gamma_3 = 0.1438996 + 0.2028538 \cdot 10^{-2}T - 0.4487672 \cdot 10^{-3}P - 0.1142945 \cdot 10^{-5}T^2 + 0.2761216 \cdot 10^{-6}P^2 \quad (22)$$

In Equations (20)–(22), the units of the temperature are Kelvin, and the units of the pressure are atmospheres. The rate constant k can be calculated from the Arrhenius expression:

$$k = A \cdot e^{\frac{-E}{R \cdot T}} \quad (23)$$

The appropriate values of the constants used in Equation (23) are listed in Table 5.

**Table 5.** Constants in the Arrhenius equation [20].

| Symbol | Name | Value | Unit |
|---|---|---|---|
| A | pre-exponential factor | $8.849 \times 10^{14}$ | kmol $m^{-3}$ $h^{-1}$ |
| E | activation energy | 40,765 | cal $mol^{-1}$ |
| R | universal gas constant | 1.987 | cal $K^{-1}$ $mol^{-1}$ |

Therefore, the formation rate of ammonia in kmol per cubic meter per hour can be written as:

$$R_{NH_3} = 1.7698 \cdot 10^{15} e^{\frac{-40765}{RT}} \left[K_a{}^2 a_1 \left(\frac{a_2{}^3}{a_3{}^2}\right)^{0.5} - \left(\frac{a_3{}^2}{a_2{}^3}\right)^{0.5}\right] \quad (24)$$

Equation (24) describes the reaction rate for catalyst particles with diameters less than 6 mm. According to Dyson and Simon [20], particles of those diameters are sufficiently small to exclude the possibility of transport and kinetic effect interaction, so no correction factor is required. However, larger particles (6–10 mm in size) are subject to diffusion restriction in their pore structure [20]. The approach to this problem is to calculate the effectiveness factor, which is a function of the conversion (η), and temperature, with pressure as a parameter [20]:

$$\xi = b_0 + b_1 T + b_2 \eta + b_3 T^2 + b_4 \eta^2 + b_5 T^3 + b_6 \eta^3 \quad (25)$$

The values of the constants $b_i$ are presented in Table 6. The pressure effect is such that higher values cause a lower effectiveness factor.

**Table 6.** Constants for the effectiveness factor (Equation (25)).

| Pressure (atm) | $b_0$ | $b_1$ | $b_2$ | $b_3$ | $b_4$ | $b_5$ | $b_6$ |
|---|---|---|---|---|---|---|---|
| 150 | −17.539096 | 0.076978 | 6.900548 | $-1.082790 \times 10^{-4}$ | −26.42469 | $4.927648 \times 10^{-8}$ | 38.93727 |
| 225 | −8.2125534 | 0.037741 | 6.190112 | $-5.354571 \times 10^{-5}$ | −20.86963 | $2.379142 \times 10^{-8}$ | 27.88403 |
| 300 | −4.6757259 | 0.023549 | 4.687353 | $-3.463308 \times 10^{-5}$ | −11.28031 | $1.540881 \times 10^{-8}$ | 10.46627 |

In Equation (25), the conversion (η) refers to the nitrogen and can be written as:

$$\eta = \frac{\dot{n}_{N_{2_{inlet}}} - \dot{n}_{N_{2_{outlet}}}}{\dot{n}_{N_{2_{inlet}}}} \quad (26)$$

where $\dot{n}_{N_{2_{inlet}}}$ is a molar flow of nitrogen at the inlet and $\dot{n}_{N_{2_{outlet}}}$ is a molar flow of nitrogen at the outlet. To summarise, for the catalyst particle size of 6–10 mm, the reaction rate can be written as:

$$R_{NH_3} = 1.7698 \cdot 10^{15} e^{\frac{-40{,}765}{RT}} \left[ {K_a}^2 a_1 \left( \frac{{a_2}^3}{{a_3}^2} \right)^{0.5} - \left( \frac{{a_3}^2}{{a_2}^3} \right)^{0.5} \right] \cdot \xi \quad (27)$$

Equations (24) and (27) are valid for the fresh catalyst, which is the assumption for the calculations. It should be noted that additional correction factors may be needed if catalyst reduction, poisoning, or ageing are considered [20].

## 3. Results

This work was focused on investigating the influence of the catalyst particle size on the ammonia synthesis in the axial-radial bed converter. For this purpose, the authors obtained the contour profiles of velocity, temperature, pressure, concentration, and reaction rate. Results received from simulations were the basis for determining the intensity of reaction among the catalyst beds and finding zones with a negligible reaction rate.

### *3.1. Flow Field*

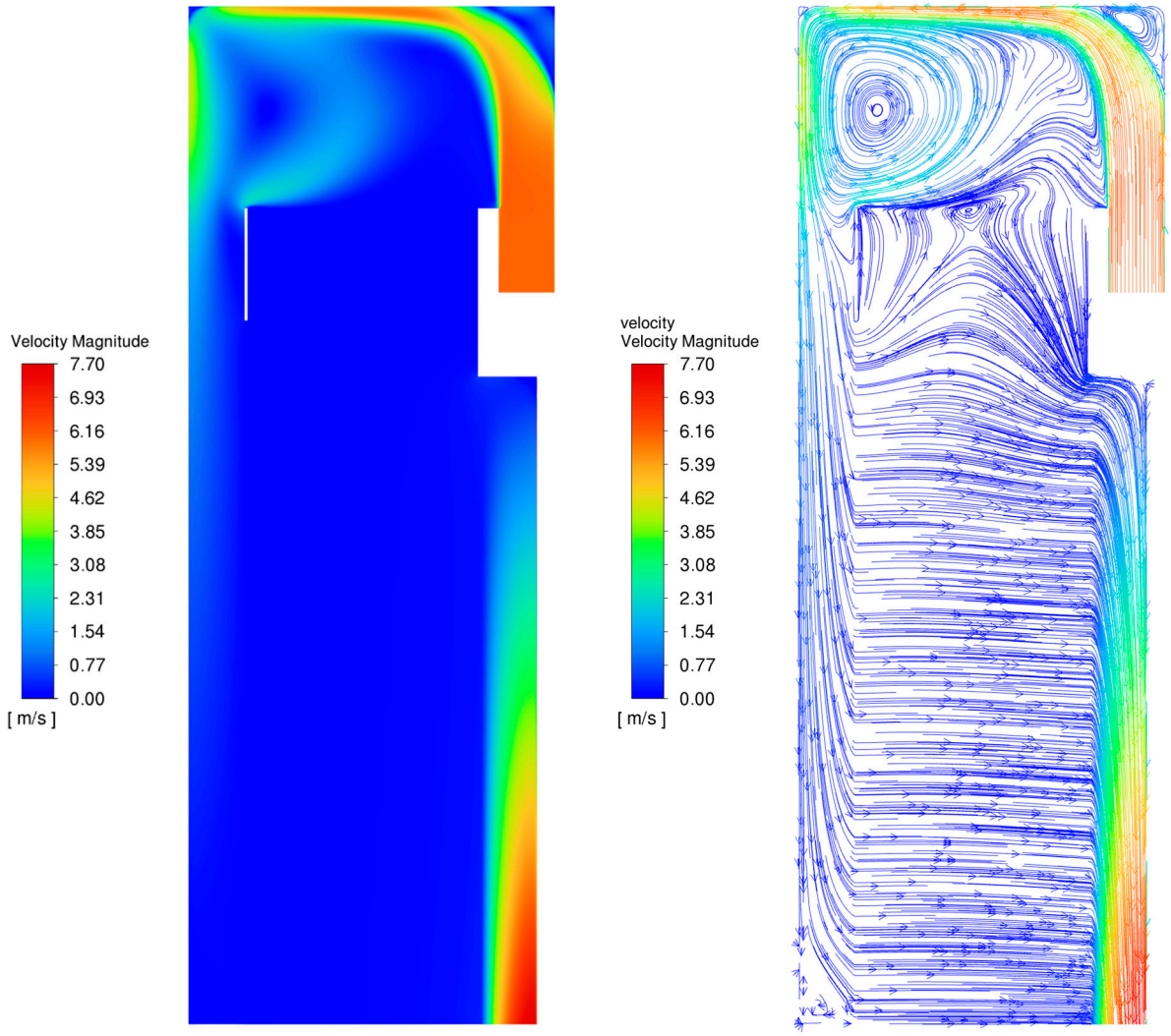
Figure 2 presents the obtained velocity contours and pathlines of the investigated geometry with a catalyst particle size of 2 mm. Velocity profiles have a similar course regardless of the size of the catalyst grains because the constant boundary condition of the reactor inlet was assumed in the calculations. Velocity profiles are the basis of most CFD simulations. This parameter directly influences mass and heat transfer. As expected, it can be seen that two "zones" of flow have formed in the bed; the upper part is dominated by axial flow, while the lower part is dominated by radial flow, which is primarily uniform. It can be observed that there is a large recirculation area in the space over the catalyst bed. The centrifugal gas inlet causes the gas flow path to curve. Part of the gas falls into the space between the outer walls of the reactor, while the rest is returned to form a vortex. In addition, there is an entrainment of part of the gas in the upper part of the catalytic bed. This causes gas to flow in different directions in the "axial-flow" part of the bed. Closer to the centre of the apparatus, the gas flows downwards towards the "radial flow" part of the bed, while in the vicinity of an outer wall of the bed, the gas flows upwards, entrained by the vortex mentioned above. The demarcation between these flows can be seen in Figure 3.

### *3.2. Catalyst Particle Size Influence*

The main aim of this work was to determine the influence of catalyst bed parameters on the process. The most evident and essential parameter is the diameter of catalyst particles. This parameter directly affects the reaction's efficiency and causes pressure losses in the flow. Smaller catalyst particles (1–2 mm diameter) are preferred in modern reactors with high activity beds [27]. Figure 4 presents the contours of the ammonia formation rate for different catalyst particle sizes, and the contours of the ammonia mole fraction are presented in Figure 5.

One can notice that the reaction is much more intense for lower values of the catalyst particle diameters (1–4 mm), especially just after the gas enters the catalyst bed. Although the reaction rate quickly lowers to negligible values. This phenomenon is caused by the fact that ammonia synthesis is a reversible reaction, and equilibrium is obtained relatively quickly. The situation differs for larger particle sizes (6–10 mm). The ammonia formation rate is much slower and occurs in the entire bed. These differences are further increased by the diffusion restriction in the particle's pore structure, which has been implemented by applying the modifier described by Equation (25). The concentration of ammonia is directly connected to the ammonia formation rate. For lower catalyst particle diameters, the ammonia concentration quickly rises and strives to be kept in equilibrium. The outlet of the catalyst bed zone contains an almost uniform concentration of ammonia for cases

with particle diameters of 1–4 mm, while for higher diameters, equilibrium is not reached before leaving the bed, which is an unwanted phenomenon.




(**a**) (**b**)

**Figure 2.** Velocity contours (**a**) and pathlines (**b**) for the investigated ammonia synthesis reactor with a catalyst particle diameter of 2 mm.

The reaction occurs in the whole volume of the catalyst bed, but its intensity is not uniform. As presented in Figure 4, there are zones in the bed where the reaction rate is very low (close to equilibrium), compared to the other part of the catalyst bed, and those differences are higher for smaller catalyst particle diameters. To show this phenomenon, we chose a value of 3% of the maximum value of the reaction rate. In this work, the part of the bed in which the reaction rate is higher than this value is treated as the "working" volume of the bed, while the remaining volume of the bed is treated as a zone with negligible reaction. This allows us to clearly present the irregularity of process intensity in the catalyst bed for different diameters of the catalyst particles. Please note that the value of 3% of the maximum value of the reaction rate is for reference only, and it can be different depending on which values of the reaction rate are considered negligible. Figure 6 presents the dependence of the "working" volume of the catalyst bed as a function of catalyst particle diameter (a) and the concentration of ammonia at the outlet of the domain as a function of catalyst particle diameter (b). Those values are firmly connected, and the highest possible

product concentration is obtained if equilibrium is reached before leaving the catalyst bed. However, if equilibrium is quickly achieved, a large portion of the bed could be redundant. This is evident in the beds with smaller catalyst particles. The proper volume of the catalyst bed should be enough to achieve equilibrium just before leaving the bed.

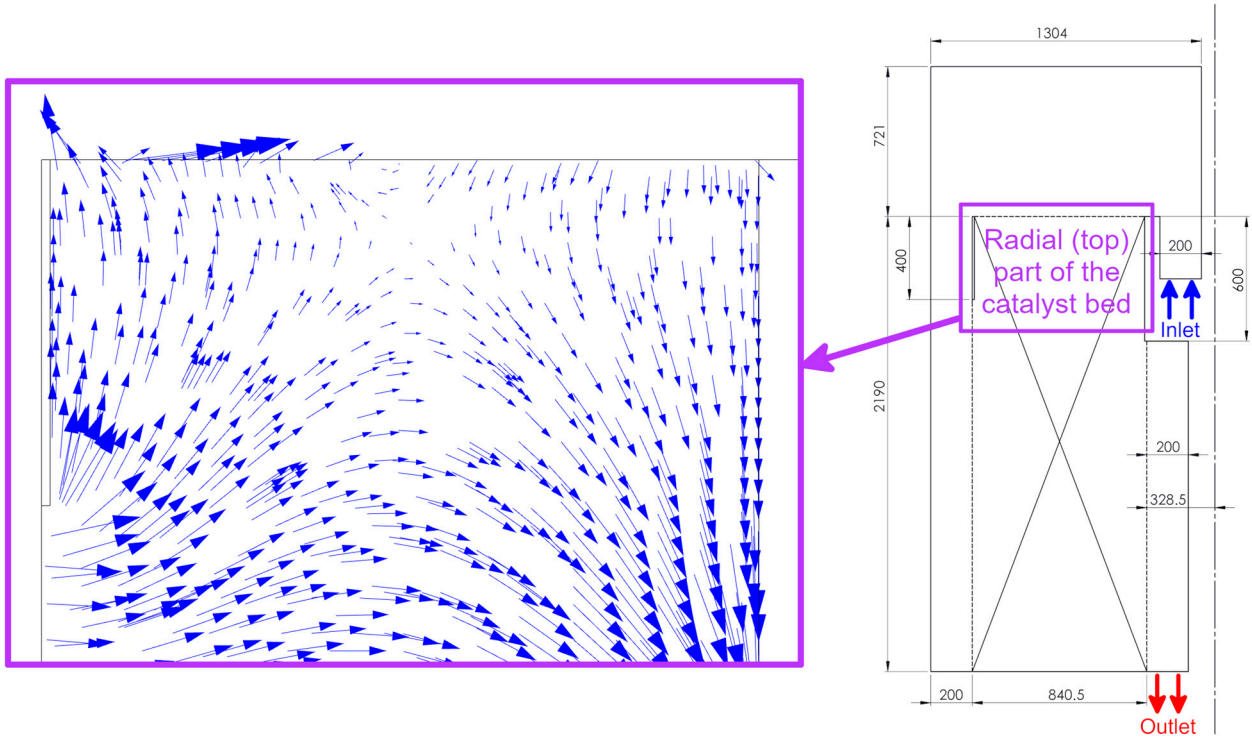



**Figure 3.** Velocity vectors in the radial (top) part of the catalyst bed in the investigated ammonia synthesis reactor with a catalyst particle diameter of 2 mm.

### *3.3. Temperature*

Ammonia synthesis is a highly exothermic reaction, which causes a strong relationship between the reaction rate and the temperature. Figure 7 presents the temperature contours. It can be noted that those contours have a similar course to the ammonia concentration contours. For a catalyst bed with lower values of particle diameters, the temperature quickly rises, and after equilibrium is reached, it becomes homogenous. The temperature growth is observed in the whole catalyst bed for the larger particle diameters.

### *3.4. Pressure Drop*

Pressure is an essential parameter for ammonia synthesis. The catalyst bed is the element that causes pressure drops during the process. This work investigated the differences in the pressure drop caused by the catalyst beds with different particle diameters. Figure 8 shows the pressure drop on the ammonia synthesis reactor's bed as a function of catalyst particle diameter. It can be observed that although the catalyst particle diameters influence the pressure drop, those values have little effect on the process due to the enormous pressure in the reactor compared to the pressure drop.

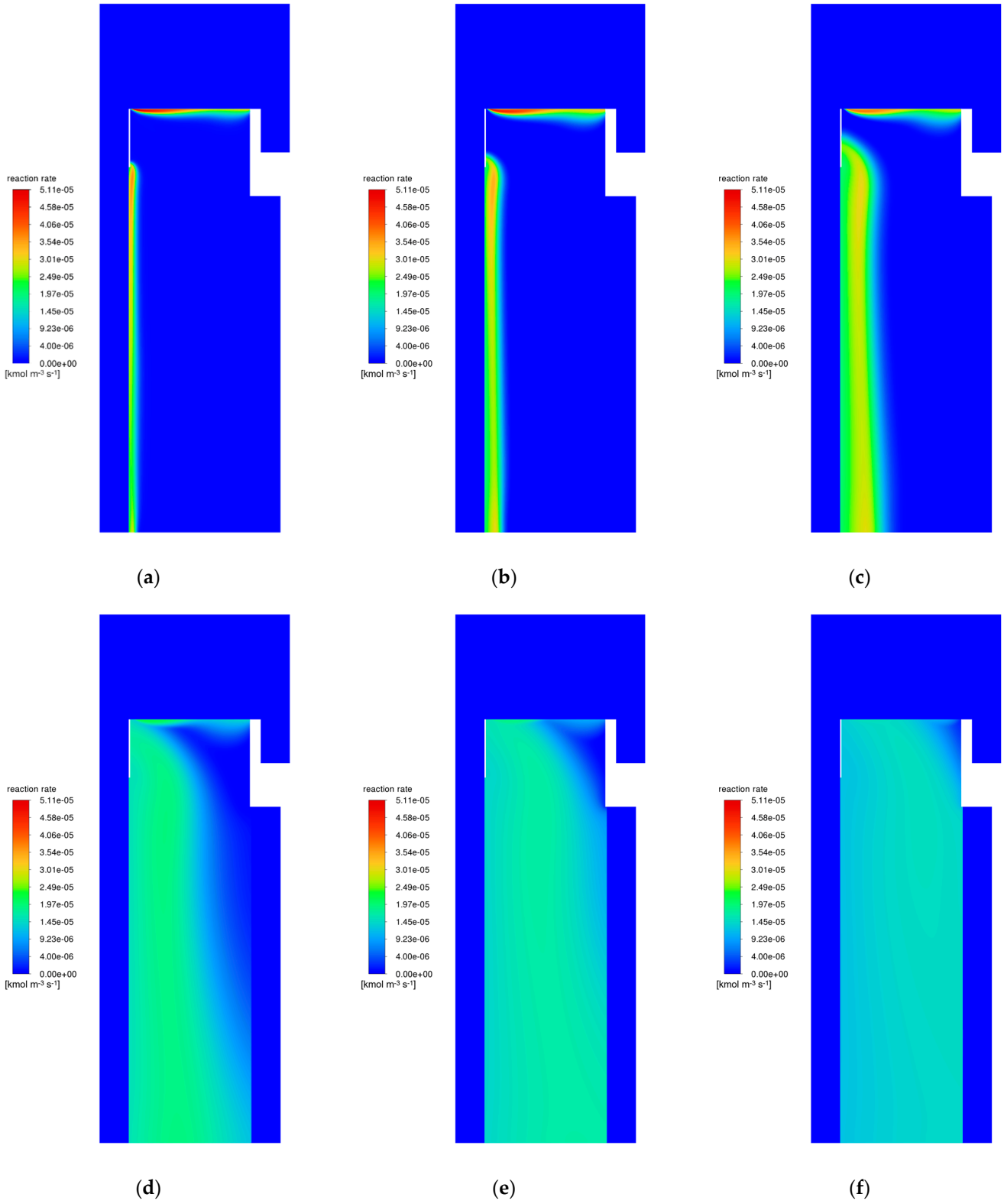



**Figure 4.** The reaction rate for the investigated ammonia synthesis reactor with a catalyst particle diameter of (**a**) 1 mm; (**b**) 2 mm; (**c**) 4 mm; (**d**) 6 mm; (**e**) 8 mm; (**f**) 10 mm. The scales of the colour maps vary.

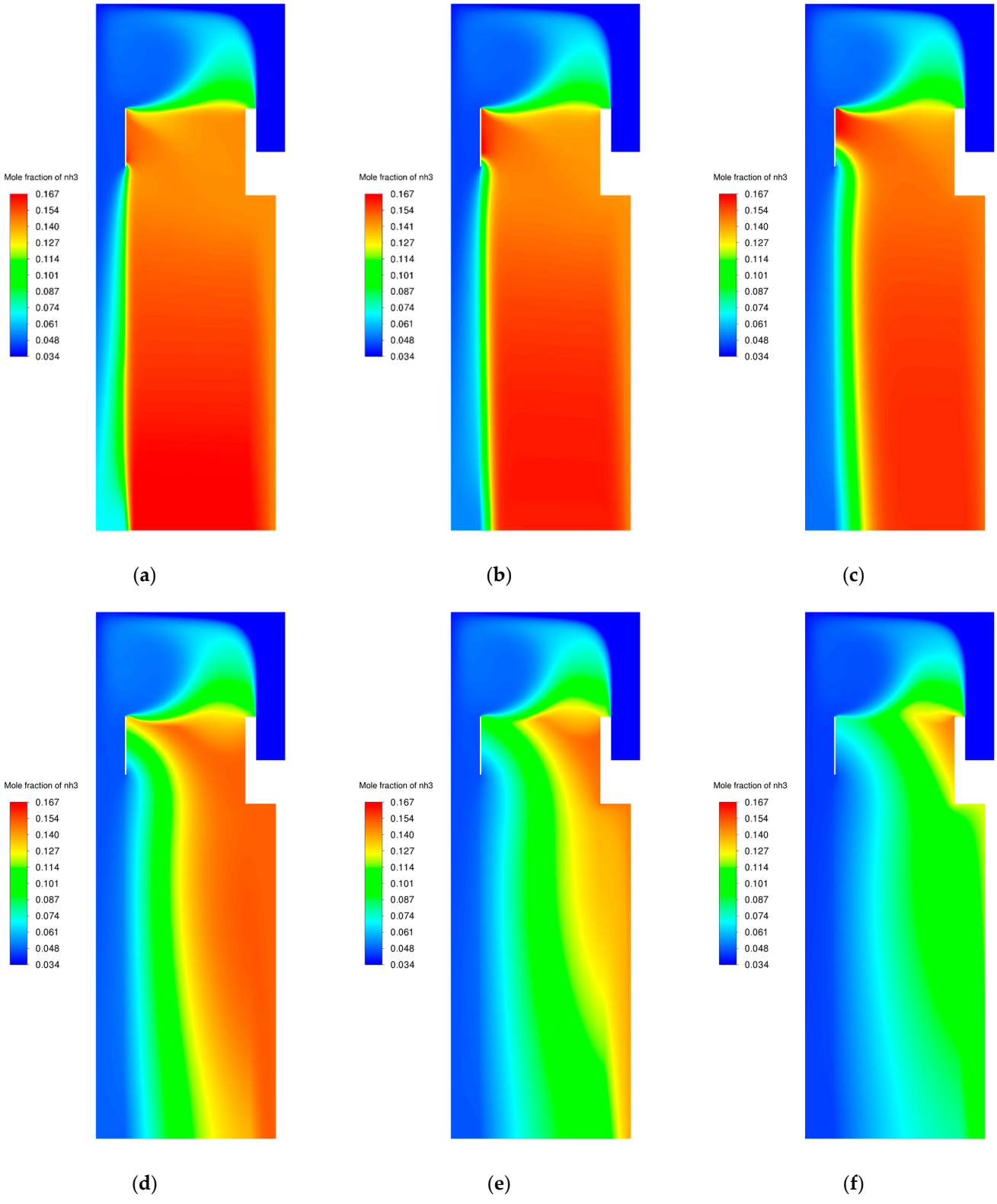
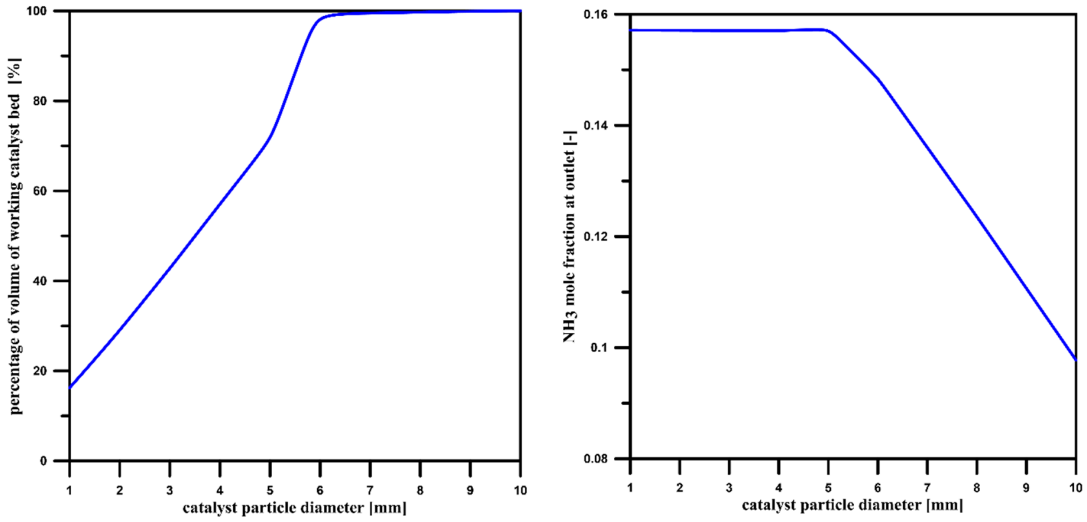
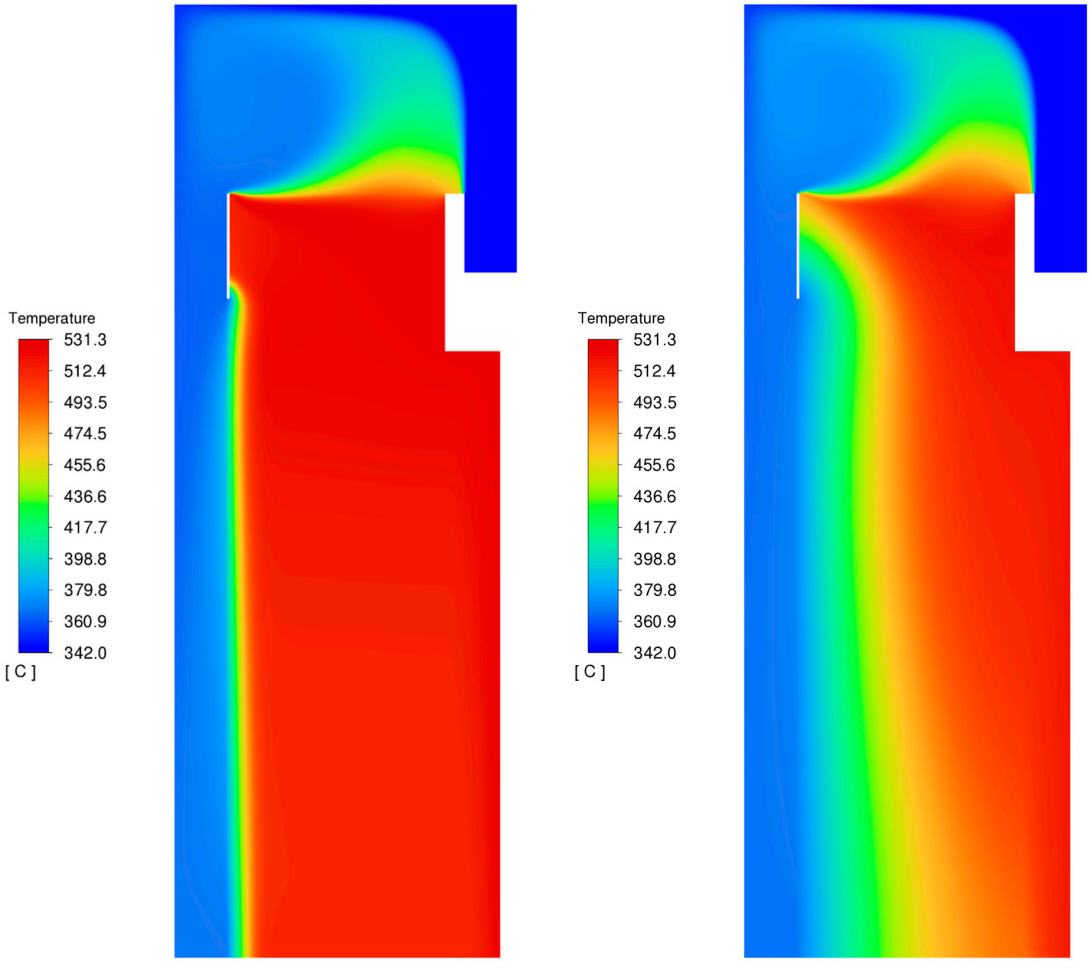



**Figure 5.** The $NH_3$ concentration contours for the investigated ammonia synthesis reactor with a catalyst particle diameter of (**a**) 1 mm; (**b**) 2 mm; (**c**) 4 mm; (**d**) 6 mm; (**e**) 8 mm; (**f**) 10 mm.




(**a**) (**b**)

**Figure 6.** The percentage of the volume of the working catalyst bed (<3% of the maximum reaction rate) (**a**) and the $NH_3$ mole fraction at the outlet (**b**) as functions of catalyst particle diameter.




(**a**) (**b**)

**Figure 7.** Temperature contours for an investigated ammonia synthesis reactor with a catalyst particle diameter of (**a**) 2 mm; (**b**) 6 mm. It can be noted that significant differences in ammonia formation rate cause differences in the maximum temperature obtained during the process.

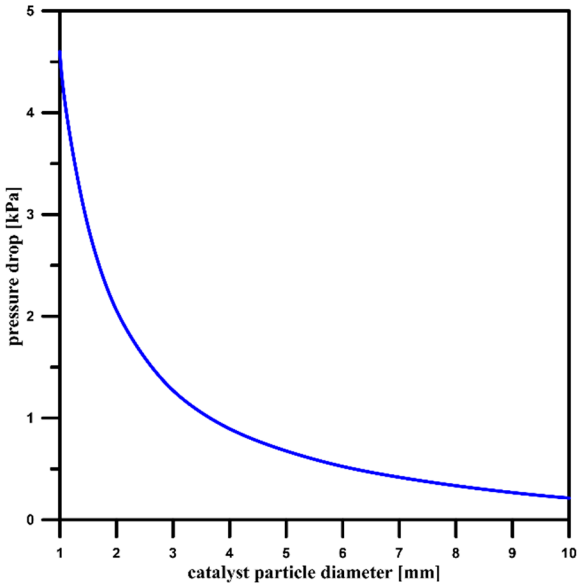



**Figure 8.** Pressure drop on the ammonia synthesis reactor's bed as a function of catalyst particle diameter.

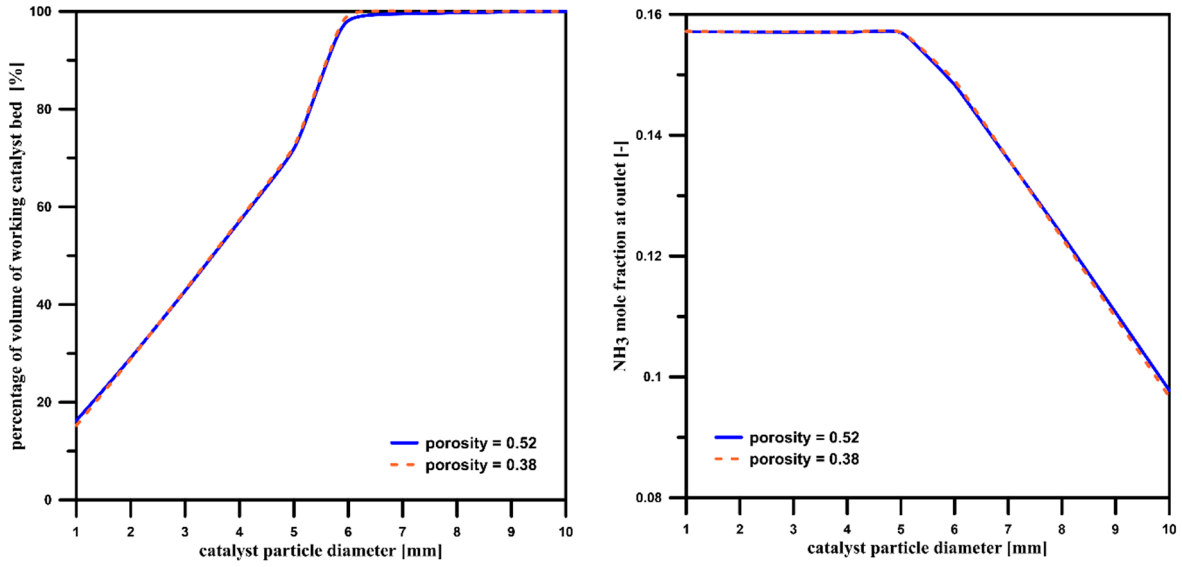
### *3.5. The Influence of the Catalyst Bed's Porosity*

The porosity of the catalyst bed (inter-particle porosity) can vary. This work used a porosity value of 0.52, which is typical for the magnetite catalyst [27]. However, this value can differ due to factors such as catalyst ageing. The porosity of an aged catalyst can drop to 0.38 [26]. In the present work, the authors compared the results using porosity values for fresh and aged catalysts. The sphericity for both catalysts is the same, and its value is 0.65. The surface-to-volume ratios for corresponding diameters also remain the same. Table 7 presents the calculated values of viscous and inertial resistances for the catalyst bed with a porosity value of 0.38. Those parameters of the catalyst bed with a porosity value of 0.52 are listed in Table 4.

**Table 7.** Calculated parameters of the catalyst bed for considered catalyst particle diameters for the bed's porosity value of 0.38.

| Particle Diameter (mm) | Viscous Resistance ($m^{-2}$) | Inertial Resistance ($m^{-1}$) |
|---|---|---|
| 1 | $1.05 \times 10^9$ | 39,547 |
| 1.5 | $4.67 \times 10^8$ | 26,364 |
| 2 | $2.63 \times 10^8$ | 19,773 |
| 3 | $1.17 \times 10^8$ | 13,182 |
| 4 | $6.57 \times 10^7$ | 9887 |
| 5 | $4.20 \times 10^7$ | 7909 |
| 6 | $2.92 \times 10^7$ | 6591 |
| 8 | $1.64 \times 10^7$ | 4943 |
| 10 | $1.05 \times 10^7$ | 3955 |

Figure 9 shows the comparison between two values of porosity (0.52 and 0.38). It can be noted that the catalyst bed's porosity has little effect on the ammonia synthesis reaction. It should be noted that only porosity is taken into account. Other factors, such as activity reduction or poisoning, require additional correction factors.




(**a**) (**b**)

**Figure 9.** The percentage of the volume of the working catalyst bed (<3% of the maximum reaction rate) (**a**) and the NH3 mole fraction at the outlet (**b**) as functions of catalyst particle diameter—comparison cases with different catalyst bed porosities.

### *3.6. Modifications of the Catalyst Bed*

There are two main challenges observed from the results presented in Section 3.2. It is necessary to reach equilibrium to achieve the highest possible ammonia concentration. However, if equilibrium is quickly reached, there is a risk that some portion of the catalyst bed will be redundant. Using CFD, it is possible to simulate the process and estimate the needed catalyst bed volume. In the investigated ammonia synthesis reactor, it can be noted that for lower catalyst particle diameters, the large part of the bed contains a negligible ammonia formation rate. The authors used CFD to simulate modified variants of catalyst beds with a catalyst particle diameter of 2 mm to find a way to quickly reduce the bed's volume without losing the process's efficiency. There are three variants of modifications with a total catalyst bed volume of about half of the original. Novel variants require only changing the geometry of the catalyst bed without altering the outer shell to make it possible to replace the bed in the existing reactor. Figure 10 presents the modified dimensions, which are listed in Table 8.

**Table 8.** Dimensions modified in novel modifications of the ammonia synthesis reactor.

| Modifications | A | B | H |
|---|---|---|---|
| original | 840.5 | 200 | 2190 |
| variant 1 | 840.5 | 200 | 1455 |
| variant 2 | 530 | 510 | 2910 |
| variant 3 | 645 | 396 | 2183 |

Figure 11 presents the ammonia formation rate contours, and Figure 12 shows the ammonia concentration contours for the proposed variants of catalyst bed geometry. Table 9 compares results between original and novel variants of the catalyst beds.

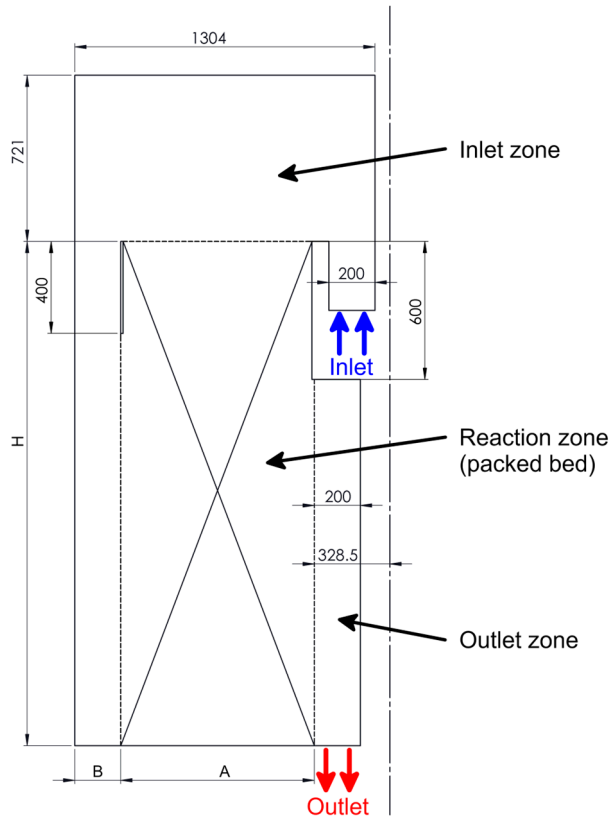
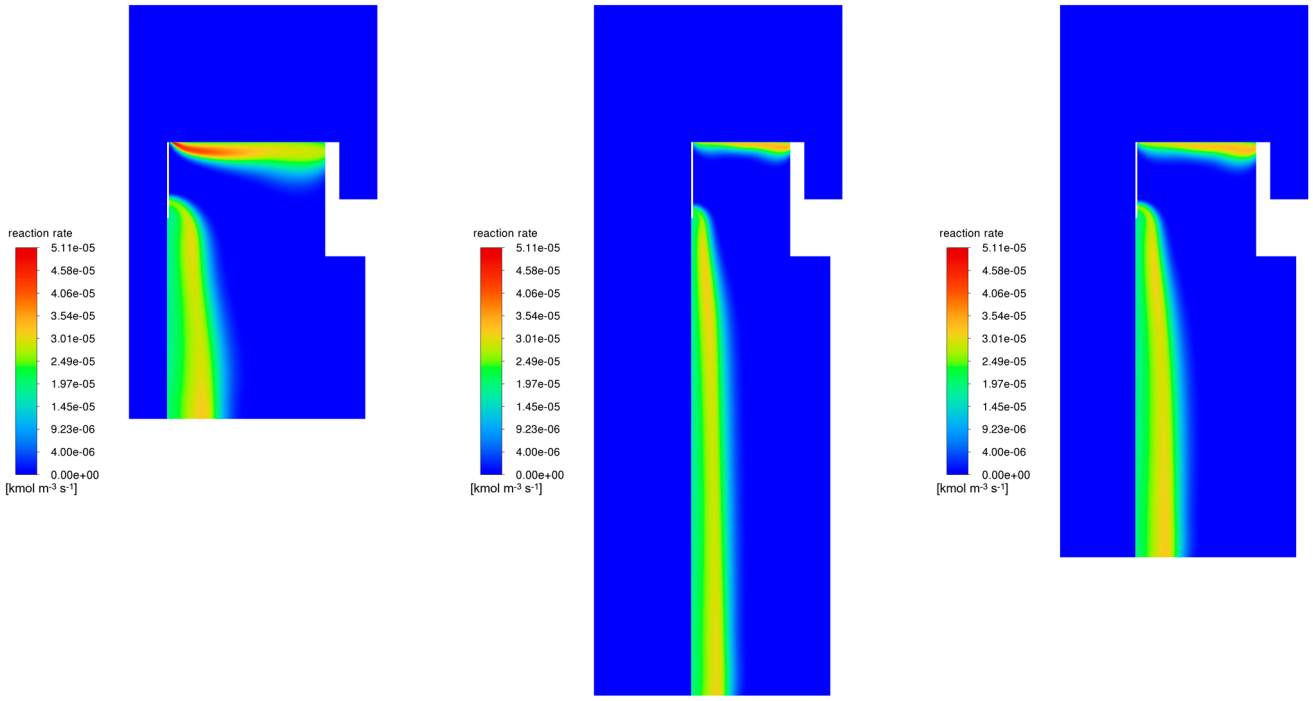
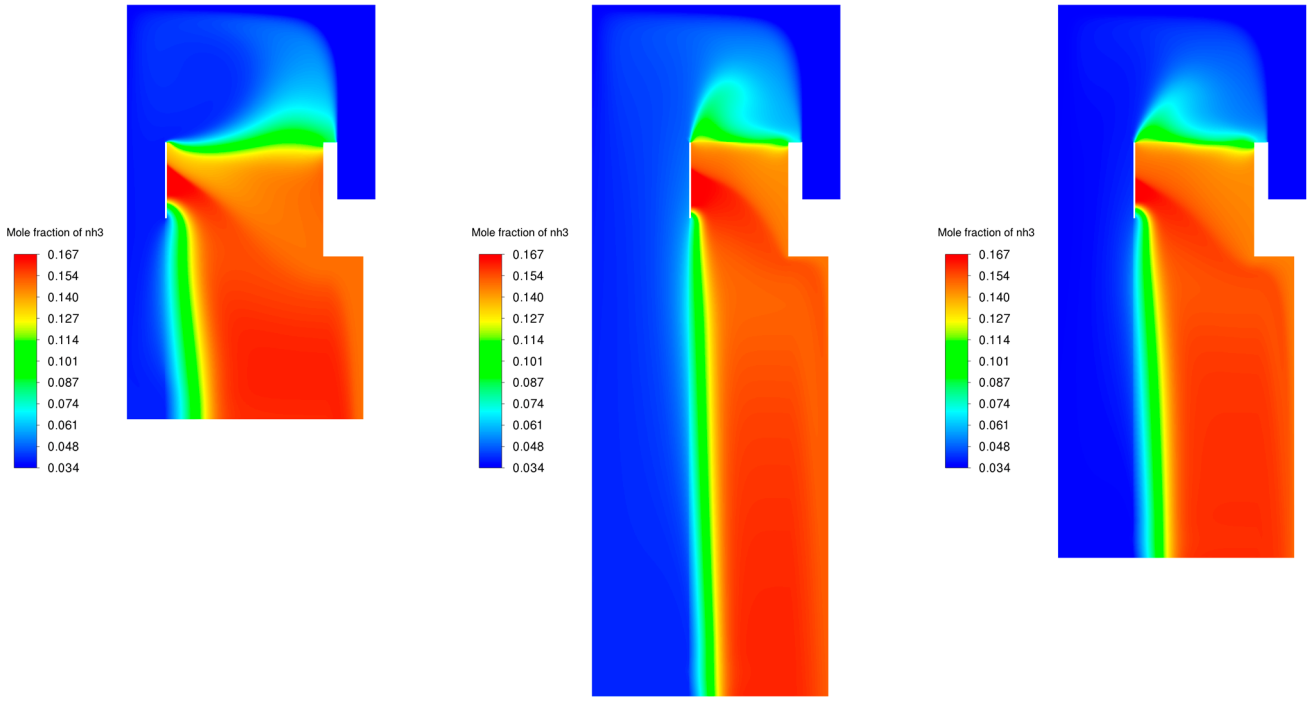



**Figure 10.** Dimensions "A", "B", and "H" are changed in modifications of the investigated ammonia converter, dimensions in mm.




(**a**) (**b**) (**c**)

**Figure 11.** The reaction rate for investigated ammonia synthesis reactor with a catalyst particle diameter of 2 mm for (**a**) variant 1; (**b**) variant 2; (**c**) variant 3.




(**a**) (**b**) (**c**)

**Figure 12.** The $NH_3$ concentration contours for the investigated ammonia synthesis reactor with a catalyst particle diameter of 2 mm for (**a**) variant 1; (**b**) variant 2; and (**c**) variant 3.

**Table 9.** Comparison of results between original and modified variants of the catalyst bed.

| Modification Variant | Catalyst Bed Volume [$m^3$] | Percentage "Working" Volume Bed [%] | $NH_3$ Mole Fraction at the Outlet [-] |
|---|---|---|---|
| original | 11.465 | 29.08 | 0.157 |
| variant 1 | 5.711 | 55.06 | 0.157 |
| variant 2 | 5.719 | 56.30 | 0.157 |
| variant 3 | 5.716 | 54.88 | 0.157 |

From the results, it can be observed that all modifications to the catalyst bed were able to maintain the efficiency of the process by reducing the bed's volume by half. The calculations show that the CFD methods can estimate the minimal amount of catalyst needed to perform the ammonia synthesis without losing efficiency. The primary benefit of reducing the volume of the catalyst bed is reducing the equipment size and potential capex. However, it should be noted that the margin for the loss of efficiency due to catalyst ageing and poisoning must be considered to allow long operation times between turnarounds, which is desirable in the industry.

### *3.7. Verification with the Literature Data*

The experimental data from Panahandeh et al. [17] was used for the verification since the process parameters and the investigated geometry of the ammonia synthesis reactor are based on the catalyst bed from this work. For the reason that the authors did not inform us about the catalyst particle diameter, we had to estimate the catalyst particle diameter based on the experimental outlet ammonia concentration [17] using the calculated relationship between the outlet ammonia fraction and catalyst particle diameter (shown in Figure 6b). The estimated value of the catalyst particle diameter is 6.8 mm. Then, using this value of the catalyst particle diameter, we conducted a simulation to calculate each other's process

parameters to compare with the experimental data given by [17]. Table 10 compares the results obtained from CFD simulation and experimental data from Panahandeh et al. [17].

**Table 10.** Comparison between calculated and experimental data.

| Parameter at the Outlet of the Catalyst Bed | Experimental Data | Calculated Data | Error [%] |
|---|---|---|---|
| $NH_3$ mole fraction [-] | 0.1403 | 0.1401 | 0.11 |
| $N_2$ mole fraction [-] | 0.1796 | 0.1796 | 0.04 |
| $H_2$ mole fraction [-] | 0.5390 | 0.5391 | 0.03 |
| $CH_4$ mole fraction [-] | 0.1035 | 0.1034 | 0.03 |
| Ar mole fraction [-] | 0.0376 | 0.0375 | 0.07 |
| temperature [°C] | 494.7 | 493.1 | 0.32 |

The results obtained are in good agreement with the data. The maximum error is about 0.11%. Due to the small error between the results, it can be concluded that the catalyst particle diameter used by [17] is correctly estimated. The proper verification of results should be sufficiently far from equilibrium. In the cases where equilibrium was reached, the concentration of ammonia (mole fraction) at the outlet was 0.1571. In the verification case (particle diameter of 6.8 mm), the concentration of ammonia at the outlet was 0.1401. This means that in the verification case, 89.2% of the equilibrium is reached.

## 4. Conclusions

This work was focused on the ammonia synthesis process in an axial-radial bed reactor. We implemented the modified Temkin-Pyzhev expression, and the examined ammonia synthesis reactor is the Topsoe converter with radial-axial flow through catalyst beds. We examined the first bed of the reactor using Computational Fluid Dynamics. Contours of velocity, temperature, pressure, concentration, and ammonia formation rate were obtained. We investigated the influence of catalyst bed parameters such as catalyst particle diameter, porosity, and pressure drop on the catalyst bed.

The obtained results show that the catalyst particle diameter has a significant influence on the process. This parameter determines how quickly equilibrium will be reached. Lower values (1–3 mm) are desired because they provide a high ammonia formation rate. We conducted the simulations for cases with different sizes of catalyst particles and estimated zones where the reaction rate is negligible. We also proposed possible bed geometry modifications to reduce bed volumes without affecting the converter's performance.

The simulation results show that relatively easy-to-make changes in the catalyst bed geometry significantly reduce the amount of catalyst bed used in the reactor. The paper shows that CFD can be a suitable tool for estimating the volume of the catalyst bed and maintaining process efficiency. It should be noted that in a real process, operational factors might limit the possible available reduction in a real ammonia production unit.

**Author Contributions:** Conceptualisation, Ł.M., M.T., J.M.B. and W.O.; methodology, Ł.M., M.T., J.M.B. and W.O.; validation, Ł.M. and M.T.; investigation, M.T. and Ł.M.; resources, Ł.M.; writing—original draft preparation, Ł.M. and M.T.; writing—review and editing, Ł.M., M.T., J.M.B. and W.O.; visualization, M.T.; supervision, Ł.M. and W.O.; project administration, Ł.M.; funding acquisition, Ł.M. All authors have read and agreed to the published version of the manuscript.

**Funding:** This research received no external funding.

**Data Availability Statement:** Not applicable.

**Conflicts of Interest:** The authors declare no conflict of interest.

## Nomenclature

The following symbols are used in this manuscript:

Latin symbols:

| | |
|---|---|
| $A$ | pre-exponential factor, kmol $m^{-3}$ $h^{-1}$ |
| $A_{fs}$ | interfacial area density (ratio of the area of the fluid-solid interface and the volume of the porous zone), $m^{-1}$ |
| $a_i$ | activity of component i |
| $b_i$ | constants |
| $C_{i,j}$,$D_{i,j}$ | prescribed matrices |
| $d_p$ | catalyst particle diameter, m |
| $C_A$ | mole fraction of component A in a plug-flow reactor |
| $C_{AL}$ | mole fraction of component A at the outlet of the plug-flow reactor |
| $C_{AL_CFD}$ | ammonia mole fraction in CFD simulation at the calculated length of the plug flow reactor |
| $C_{A0}$ | mole fraction of component A at the inlet of a plug-flow reactor |
| $C_1$ | viscous resistance, $m^{-2}$ |
| $C_2$ | inertial resistance factor, $m^{-1}$ |
| $E$ | activation Energy, cal $mol^{-1}$ |
| $E_f$ | total fluid energy, J |
| $E_s$ | total solid medium energy, J |
| $f_i$ | fugacity of component i in a mixture |
| $f_i^*$ | fugacity of component i at standard state |
| $f_i^0$ | fugacity of a pure component i at temperature and pressure of the system |
| $F_2$ | parameter |
| $G_b$ | generation of turbulence kinetic energy due to buoyancy |
| $G_k$ | generation of turbulence kinetic energy due to the mean velocity gradients |
| $G_\omega$ | generation of specific dissipation rates due to the mean velocity gradients |
| $G_{\omega b}$ | generation of specific dissipation rate due to buoyancy |
| $h_i$ | enthalpy of the component i, J $kg^{-1}$ |
| $h_{fs}$ | heat transfer coefficient for the fluid-solid interface, W $m^{-2}$ $K^{-1}$ |
| $I$ | unit tensor |
| $\vec{J}_i$ | diffusion flux of species i, kg $m^{-2}$ $s^{-1}$ |
| $k$ | reaction rate constant, $s^{-1}$ |
| $k$ | turbulent kinetic energy, $m^2$ $s^{-2}$ |
| $K_a$ | equilibrium constant in terms of activities |
| $k_f$ | fluid phase thermal conductivity, W $m^{-1}$ $K^{-1}$ |
| $k_s$ | solid medium thermal conductivity, W $m^{-1}$ $K^{-1}$ |
| $L$ | length of the plug-flow reactor, m |
| $\dot{n}_{N_{2_{inlet}}}$ | molar flow of nitrogen at the inlet, kmol $s^{-1}$ |
| $\dot{n}_{N_{2_{outlet}}}$ | molar flow of nitrogen at the outlet, kmol $s^{-1}$ |
| $P$ | pressure, Pa, atm |
| $R$ | universal gas constant cal $K^{-1}$ $mol^{-1}$ |
| $r_A$ | the formation rate of component A in a plug-flow reactor |
| $R_i$ | net rate of production of species i by chemical reaction |
| $R_{NH_3}$ | ammonia formation rate, kmol $m^{-3}$ $s^{-1}$ |
| $S$ | strain rate magnitude, $s^{-1}$ |
| $S_i$ | rate of creation of species i by addition from the dispersed phase plus any user-defined sources |
| $S_i$ | source term for the i (x, y, or z) momentum equation |
| $S_k$ | user-defined source term of turbulence kinetic energy |
| $S_v$ | surface-to-volume ratio, $m^{-1}$ |
| $S_\omega$ | user-defined source term for a specific dissipation rate |
| $S_f^h$ | fluid enthalpy source term |
| $S_s^h$ | solid enthalpy source term |
| $T$ | temperature, °C, K |
| $t$ | time, s |
| $T_f$ | temperature of the fluid, K |
| $T_s$ | temperature of the solid medium, K |
| $u$ | continuous phase velocity, m $s^{-1}$ |
| $u_i$, $v_i$ | continuous phase velocity in the i direction, m $s^{-1}$ |

| | |
|---|---|
| $u\prime$ | average fluctuation of continuous phase velocity, m $s^{-1}$ |
| $\|v\|$ | magnitude of velocity, m $s^{-1}$ |
| $\vec{v}$ | overall velocity vector, m $s^{-1}$ |
| $x_i$, $x_j$ | computational domain dimensions, m |
| y | distance, m |
| $y^+$ | dimensionless wall distance |
| $y_i$ | mole fraction of component i |
| $Y_i$ | local mass fraction of species i |
| $Y_k$ | dissipation of turbulence kinetic energy due to turbulence |
| $Y_\omega$ | dissipation of a specific dissipation rate due to turbulence |
| Greek symbols: | |
| $\alpha$ | parameter |
| $\alpha$ | permeability, $m^2$ |
| $\alpha^*$, $\alpha_1$ | coefficients |
| $\gamma_i$ | activity coefficient of component i |
| $\varepsilon$ | porosity of the medium |
| $\eta$ | conversion |
| $\mu$ | continuous phase dynamic viscosity, Pa·s |
| $\mu_t$ | continuous phase turbulent viscosity, Pa·s |
| $\xi$ | effectiveness factor |
| $\rho$ | continuous phase density, kg $m^{-3}$ |
| $\rho_f$ | fluid denstity, kg $m^{-3}$ |
| $\rho_s$ | solid medium density, kg $m^{-3}$ |
| $\sigma_k$ | turbulent Prandtl number for k |
| $\sigma_\omega$ | turbulent Prandtl number for $\omega$ |
| $\psi$ | sphericity |
| $\omega$ | specific dissipation rate, $s^{-1}$ |
| Acronyms: | |
| CFD | Computational Fluid Dynamics |
| SIMPLE | Semi-Implicit Method for Pressure-Linked Equations |

## References


1. Hoque, A.; Mohiuddin, M.; Su, Z. Effects of Industrial Operations on Socio-Environmental and Public Health Degradation: Evidence from a Least Developing Country (LDC). *Sustainability* **2018**, *10*, 3948. [CrossRef]
2. Klumpp, A.; Domingos, M.; Klumpp, G. Assessment of the Vegetation Risk by Fluoride Emissions from Fertiliser Industries at Cubatão, Brazil. *Sci. Total Environ.* **1996**, *10*, 219–228. [CrossRef]
3. Roser, M.; Ritchie, H. Hunger and Undernourishment. Available online: https://ourworldindata.org/hunger-and-undernourishment (accessed on 14 September 2022).
4. Global Market Insights Fertilizer Market Size, Share & Forecasts 2022–2030. Available online: https://www.gminsights.com/industry-analysis/fertilizer-market (accessed on 11 May 2023).
5. Maximize Market Research Water Soluble Fertilizer Market: Increasing Acceptance of Micro-Irrigation Practices Is Expected to Drive the Market. Available online: https://www.maximizemarketresearch.com/market-report/global-water-soluble-fertilizer-market/33171/ (accessed on 11 May 2023).
6. Research and Markets ltd Fertilizer Market: Global Industry Trends, Share, Size, Growth, Opportunity and Forecast 2023–2028. Available online: https://www.researchandmarkets.com/reports/5768989/fertilizer-market-global-industry-trends (accessed on 11 May 2023).
7. Statista Fertilizer Industry Worldwide. Available online: https://www.statista.com/study/106183/global-fertilizer-industry/ (accessed on 9 May 2023).
8. Ritchie, H. To Protect the World's Wildlife We Must Improve Crop Yields—Especially across Africa. Available online: https://ourworldindata.org/yields-habitat-loss (accessed on 9 May 2023).
9. Modak, J.M. Haber Process for Ammonia Synthesis. *Resonance* **2011**, *16*, 9. [CrossRef]
10. Schlögl, R. Ammonia Synthesis. In *Handbook of Heterogeneous Catalysis 8 Volume Set*, 2nd ed.; Wiley: New York, NY, USA, 2008; Volume 5, pp. 2501–2575. ISBN 978-3-527-31241-2.
11. Tamaru, K. The History of the Fevelopment of Ammonia Synthesis. In *Catalytic Ammonia Synthesis: Fundamentals and Practice*; Fundamental and Applied Catalysis; Springer: Boston, MA, USA, 1991; ISBN 978-1-4757-9594-3.
12. Hooper, C.W. Ammonia Synthesis: Commercial Practice. In *Catalytic Ammonia Synthesis: Fundamentals and Practice*; Fundamental and Applied Catalysis; Springer: Boston, MA, USA, 1991; ISBN 978-1-4757-9594-3.
13. Singh, C.P.P.; Saraf, D.N. Simulation of Ammonia Synthesis Reactors. *Ind. Eng. Chem. Proc. Des. Dev.* **1979**, *18*, 364–370. [CrossRef]

14. Jorqueira, D.S.S.; Neto, A.M.B.; Rodrigues, M.T.M. Modeling and Numerical Simulation of Ammonia Synthesis Reactors Using Compositional Approach. *ACES* **2018**, *8*, 124–143. [CrossRef]
15. Elnashaie, S.S.E.H.; Mahfouz, A.T.; Elshishini, S.S. Digital Simulation of an Industrial Ammonia Reactor. *Chem. Eng. Process. Process. Intensif.* **1988**, *23*, 165–177. [CrossRef]
16. Kasiri, N.; Hosseini, A.R.; Moghadam, M. Dynamic Simulation of an Ammonia Synthesis Reactor. In *Computer Aided Chemical Engineering*; Elsevier: Amsterdam, The Netherlands, 2003; Volume 14, pp. 695–700. ISBN 978-0-444-51368-7.
17. Panahandeh, M.R.; Fathikaljahi, J.; Taheri, M. Steady-State Modeling and Simulation of an Axial-Radial Ammonia Synthesis Reactor. *Chem. Eng. Technol.* **2003**, *26*, 666–671. [CrossRef]
18. Dashti, A.; Khorsand, K.; Marvast, M.A.; Kakavand, M. Modeling and Simulation of Ammonia Synthesis Reactor. *Petroleum and Coal* **2006**, *48*, 15–23.
19. Azarhoosh, M.J.; Farivar, F.; Ale Ebrahim, H. Simulation and Optimization of a Horizontal Ammonia Synthesis Reactor Using Genetic Algorithm. *RSC Adv.* **2014**, *4*, 13419–13429. [CrossRef]
20. Dyson, D.C.; Simon, J.M. Kinetic Expression with Diffusion Correction for Ammonia Synthesis on Industrial Catalyst. *Ind. Eng. Chem. Fund.* **1968**, *7*, 605–610. [CrossRef]
21. Mirvakili, A.; Eksiri, Z.; Biniaz, P.; Mohaghegh, N. Two-Dimensional Mathematical Modeling of an Industrial Ammonia Synthesis Reactor with CFD Analysis. *J. Taiwan Inst. Chem. Eng.* **2021**, *121*, 1–19. [CrossRef]
22. Araújo, A.; Skogestad, S. Control Structure Design for the Ammonia Synthesis Process. *Comput. Chem. Eng.* **2008**, *32*, 2920–2932. [CrossRef]
23. Jaymes Dionne, C.; Gutowska, I.; Brian Jackson, R. CFD Simulations to Characterize near Wall Heat Transfer in High Prandtl Number Packed Bed Conditions. *Nucl. Eng. Des.* **2022**, *396*, 111868. [CrossRef]
24. Lee, J.-J.; Yoon, S.-J.; Park, G.-C.; Lee, W.-J. Turbulence-Induced Heat Transfer in PBMR Core Using LES and RANS. *J. Nucl. Sci. Technol.* **2007**, *44*, 985–996. [CrossRef]
25. *Ansys® Fluent, Release 2021 R2, Help System, Fluent Theory Guide*; ANSYS, Inc.: Canonsburg, PA, USA, 2021.
26. Gramatica, G.; Pernicone, N. Kinetics of Ammonia Synthesis and Influence on Converter Design. In *Catalytic Ammonia Synthesis: Fundamentals and Practice*; Fundamental and Applied Catalysis; Springer: Boston, MA, USA, 1991; ISBN 978-1-4757-9594-3.
27. Tennison, S.R. Alternative Noniron Catalysts. In *Catalytic Ammonia Synthesis: Fundamentals and Practice*; Fundamental and Applied Catalysis; Springer: Boston, MA, USA, 1991; ISBN 978-1-4757-9594-3.
28. Gillespie, L.J.; Beattie, J.A. The Thermodynamic Treatment of Chemical Equilibria in Systems Composed of Real Gases. I. An Approximate Equation for the Mass Action Function Applied to the Existing Data on the Haber Equilibrium. *Phys. Rev.* **1930**, *36*, 743–753. [CrossRef]


**Disclaimer/Publisher's Note:** The statements, opinions and data contained in all publications are solely those of the individual author(s) and contributor(s) and not of MDPI and/or the editor(s). MDPI and/or the editor(s) disclaim responsibility for any injury to people or property resulting from any ideas, methods, instructions or products referred to in the content.